



Prediction of the radiated sound power from a fluid-loaded finite cylinder using the surface contribution method

Daipei LIU¹; Herwig PETERS¹; Nicole KESSISSOGLU¹; Steffen MARBURG²;

¹ School of Mechanical and Manufacturing Engineering, UNSW Australia, Sydney, NSW 2052, Australia

² LRT4-Institute of Mechanics, Universität der Bundeswehr München, D-85579 Neubiberg, Germany

ABSTRACT

Based on acoustic radiation modes, the surface contribution method has been developed to predict the surface contributions to the radiated sound power from a vibrating structure. In this work, the surface contribution method is used to identify the sound field on a vibrating structure submerged in a heavy fluid. It was recently found that surface contribution method was not able to predict the surface contributions at low frequencies when the structural wavenumber is higher than the acoustic wavenumber. In this paper, the acoustic radiation efficiencies calculated for different numbers of integration points are compared and used to compute the surface contributions to the radiated sound power. The radiated sound power obtained from both the surface contribution and the active intensity methods are compared. Numerical results for a fully coupled finite element/boundary element model of a cylindrical shell with hemispherical end closures submerged in water show that the surface contribution method can also be successfully applied at low frequencies.

Keywords: Surface contribution method, acoustic radiation efficiencies, active intensity, supersonic acoustic intensity I-INCE Classification of Subjects Number(s): 51.4

1. INTRODUCTION

For many transportation noise problems, a main focus is on the prediction of the structure-borne noise due to engine and gearbox vibration. In particular, predicting the vibro-acoustic responses of a vibrating structure immersed in a fluid is significant for both design purposes and application of noise control in maritime vessels. Several techniques to predict exterior radiated sound from vibrating structures have been developed and are described as follows. Acoustic radiation modes are a set of orthogonal surface velocity distributions of a vibrating structure, which were first introduced by Borgiotti (1) for exterior radiation problems. The acoustic radiation efficiency is associated to each radiation mode and the corresponding radiated power for each acoustic radiation mode is completely independent from the power of other acoustic radiation modes. The total radiated sound power is the sum of all radiated powers generated by each acoustic mode. Using singular value decomposition, Borgiotti (1) found that the boundary velocity patterns can be divided into observable and non-observable components. The observable components have high radiation efficiencies from a subset of velocity patterns, which depends on the dimension of the object and size in wavelengths, while the non-observable components do not radiate efficiently and contribute mainly to the near field of the object. The radiation problem can also be explored using a wave vector filtering approach (2), which was shown to provide insight into the nature of the coupling between a vibrating structure and its accompanying radiated field. The relationship between singular value decomposition and a wave vector filtering method to compute radiated sound was presented by Photiadis (3). Sarkissian (4) calculated the acoustic radiation modes by eigenstates of the real part of the surface impedance operator, which were shown to be equal to those calculated using singular value decomposition. Cunefare and Currey (5) found that sufficient degrees of freedom of the acoustic modes must be used to ensure convergence of radiation efficiencies. The radiation efficiency of the most efficient acoustic mode has a finite upper bound and is the quickest to converge. Snyder and Tanaka (6) presented a technique to determine the total acoustic power using modal radiation efficiencies. The acoustic radiated power of a simply supported rectangular plate at low frequencies was calculated. The accuracy of the calculated sound power was shown to depend on the accuracy of each individual acoustic efficiency.

¹daipei.liu@student.unsw.edu.au

Based on acoustic radiation modes, Marburg et al. (7) presented a new method to predict the radiated sound power based on the surface contributions of a vibrating structure. Eigenvalue decomposition was used to calculate the acoustic radiation modes and acoustic radiation efficiency. The surface contribution was calculated based on the acoustic radiation modes, acoustic radiation efficiencies and either acoustic pressure or normal structural velocity. Similar to the concept of the surface contribution method, Williams (8) developed a set of formulae based on spatial convolution, which only require either pressure or velocity and described non-negative intensity. The non-negative intensity of a point driven plate was compared to the supersonic acoustic intensity method, also developed by Williams (9, 10). The results obtained using either method showed almost the same results. However, Williams (8) found that the non-negative intensity could not localize the source at frequencies below the coincidence frequency. At lower frequencies, supersonic acoustic intensity based on the wavenumber filtering method was shown to increase resolution and successfully locate the radiation hot spots (10).

The purpose of this paper is to extend the study of the surface contribution method with application to a cylinder. A fully coupled finite element/boundary element model of a cylindrical shell with hemispherical end closures is developed. A focus of this work is to examine the surface contribution method at low frequencies, when the structural wavenumber is higher than the acoustic wavenumber. The surface contributions are derived from a hypothetical surface field determined by the eigenvalues, acoustic radiation modes and particle velocity. The acoustic radiation efficiencies based on different discretizations and integration points are compared to examine the surface contributions. To verify the surface contribution method, the radiated sound power of the first three bending modes computed from both the surface contribution and active intensity methods are compared.

2. METHODOLOGY

2.1 Sound intensity and sound power

Complex sound intensity on a structural surface can be separated into its active and reactive components (8). The active component is the energy radiated to the far field, while the reactive component only contributes to instantaneous power radiation that vanishes when averaged over a period. After collocation and Galerkin discretization using the boundary element method, the radiated sound power is the sum of all nodal sound power contributions. The active acoustic intensity is defined by

$$\mathbf{I} = \frac{1}{2} \Re \{ p \mathbf{v}^* \} \quad (1)$$

where p is the acoustic pressure, \mathbf{v} is the particle velocity and $()^*$ denotes the complex conjugate. The particle velocity is calculated by (11)

$$\mathbf{v} = i\omega \mathbf{C}_{fs} \mathbf{u} \quad (2)$$

where ω is the angular frequency, \mathbf{C}_{fs} is a fluid-structure coupling matrix and \mathbf{u} is the nodal displacement vector (12). The radiated sound power is defined as (13)

$$P = \int_{\Gamma} \mathbf{I} \cdot \mathbf{n} d\Gamma \quad (3)$$

where Γ is the boundary contour of the exterior acoustic domain and \mathbf{n} is the normal direction on Γ .

2.2 Acoustic radiation efficiency

The acoustic radiation efficiency is defined as the ratio of radiated sound power and the reference sound power (14, 15). The reference sound power P_{ref} is defined as

$$P_{\text{ref}} = \frac{1}{2} \Re \left\{ \int_{\Gamma} \bar{p} \bar{v}^* d\Gamma(\mathbf{x}) \right\} = \frac{1}{2} \Re \{ S \bar{p} \bar{v}^* \} \quad (4)$$

where S is the surface area of the radiator and \bar{v} is the spatially averaged mean velocity of the normal components of the velocity of the surface. After using the specific acoustic impedance $z = p/v = \rho_0 c$, the radiation efficiency can be expressed as (16)

$$\sigma = \frac{P}{P_{\text{ref}}} = \frac{2P}{\rho_0 c \Re \{ S \bar{v}^* \}} \quad (5)$$

Equation (5) leads to the generalized eigenvalue problem of the resistive acoustic impedance matrix \mathbf{Z}_R and the boundary mass matrix \mathbf{M} . The diagonal matrix of the eigenvalues $\mathbf{\Lambda}$ and the eigenvector matrix $\mathbf{\Psi}$ can be

calculated by eigenvalue decomposition (7). Using the eigenvalue matrix, the radiation efficiency σ can be shown to be (16)

$$\sigma = \frac{\lambda_l}{\rho_0 c} \quad (6)$$

where λ_l are the eigenvalues.

2.3 Surface contributions to the radiated sound power

As the surface contributions to the radiated sound power are always positive, the total radiated sound power can be expressed in terms of the sum of the surface contributions η through the total boundary surface (7)

$$P = \frac{1}{2} \int_{\Gamma} \eta(\mathbf{x}) d\Gamma(\mathbf{x}) = \frac{1}{2} \int_{\Gamma} \beta(\mathbf{x}) \beta^*(\mathbf{x}) d\Gamma(\mathbf{x}) \quad (7)$$

The physical unit of η is [W/m²]. Using the boundary mass matrix Θ defined as (16)

$$\Theta = \int_{\Gamma} \phi \phi^{\top} d\Gamma \quad (8)$$

to discretize the boundary surface integral, $\beta(\mathbf{x})$ can be expressed as

$$\beta(\mathbf{x}) = \phi^{\top}(\mathbf{x}) \boldsymbol{\beta} \quad (9)$$

where ϕ is a column matrix. $\boldsymbol{\beta}$ is a vector without physical significance and can be computed using the eigenvector matrix Ψ , the eigenvalue matrix Λ , the boundary mass matrix Θ and normal velocity vector \mathbf{v} as follows (7)

$$\boldsymbol{\beta} = \Psi \sqrt{\Lambda} \Psi^{\top} \Theta \mathbf{v} \quad (10)$$

3. RESULTS

The boundary element code AKUSTA (17) is used to implement the surface contribution method to a structure of a cylindrical shell with hemispherical end closures and submerged in a heavy fluid medium. Constant discontinuous boundary elements have been used for this model. Two different sets of integration points per element are used to examine the surface contribution method at low frequencies. The number of integration points in each set is based on the ratio between the distance from the collocation point to the element and the size of the element (18). Figure 1 shows that as the distance between the collocation point and the element increases, the number of integration points in set A reduces by steps from 30 to 2, while the numbers in set B are always 30.

A harmonic analysis using ring force excitation at one end of the cylinder, corresponding to the junction between the cylindrical and hemispherical shells at the bottom end, is initially conducted. The cylindrical shell is 45 m long with 6.5 m diameter. Including the hemispherical end caps, the total length is 51.5 m. The structure is modelled with 144 elements for coarse discretization and 576 elements for fine discretization. Density of $\rho = 1000 \text{ kg/m}^3$ and speed of sound of $c = 1482 \text{ m/s}$ are assumed for water. Damping exists in the form of radiation damping. Velocity distribution patterns are obtained according to certain selected mode shapes. After the velocity distribution patterns are selected, a modal analysis is then conducted by increasing the frequency for the chosen velocity distribution pattern in order to observe the acoustic intensity and surface contributions at different frequencies.

The particle velocity pattern of the third bending mode is used to compare the distribution differences of the active acoustic intensity \mathbf{I} and the surface contribution η at different frequencies. The first column of Figure 2 shows the particle displacement \mathbf{u} of the third bending mode. The second to the fifth columns respectively show the real and imaginary parts of the particle velocity and sound pressure. The sixth and seventh columns respectively present the active acoustic intensity and surface contribution. In Figure 2(a), the real and imaginary parts of the particle velocity and sound pressure show the same radiation pattern. The radiating patterns of the active acoustic intensity and the surface contribution are notably different at the lower frequency of 1 Hz. The active acoustic intensity on most sections of the surface is almost zero, except close to the excitation location which indicates the maximum radiation energy. In contrast, the surface contribution shows a distribution where a large area of the cylinder is significantly contributing to the radiated sound. Figure 2(b) presents similar results to that in Figure 2(a) for the particle velocity, sound pressure, active intensity and surface contribution, for the same bending mode but at a higher frequency of 100 Hz. The active acoustic intensity and the surface contribution now have a similar radiation pattern. This is due to the decreased wavelength which makes it

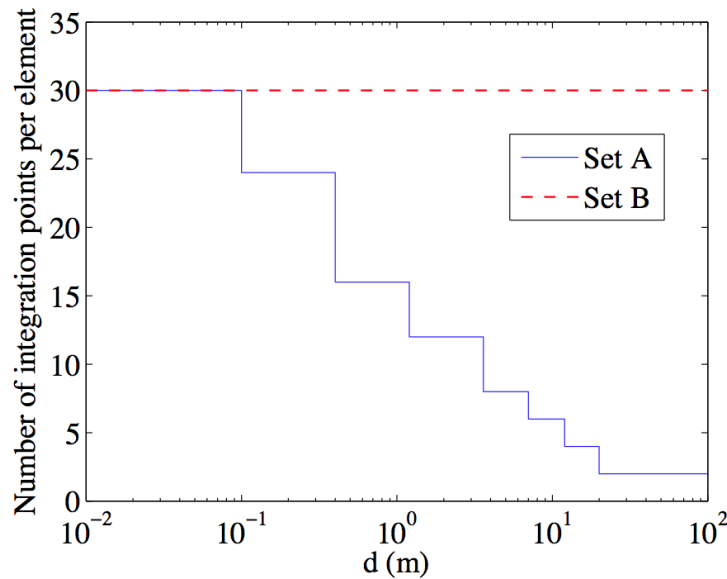


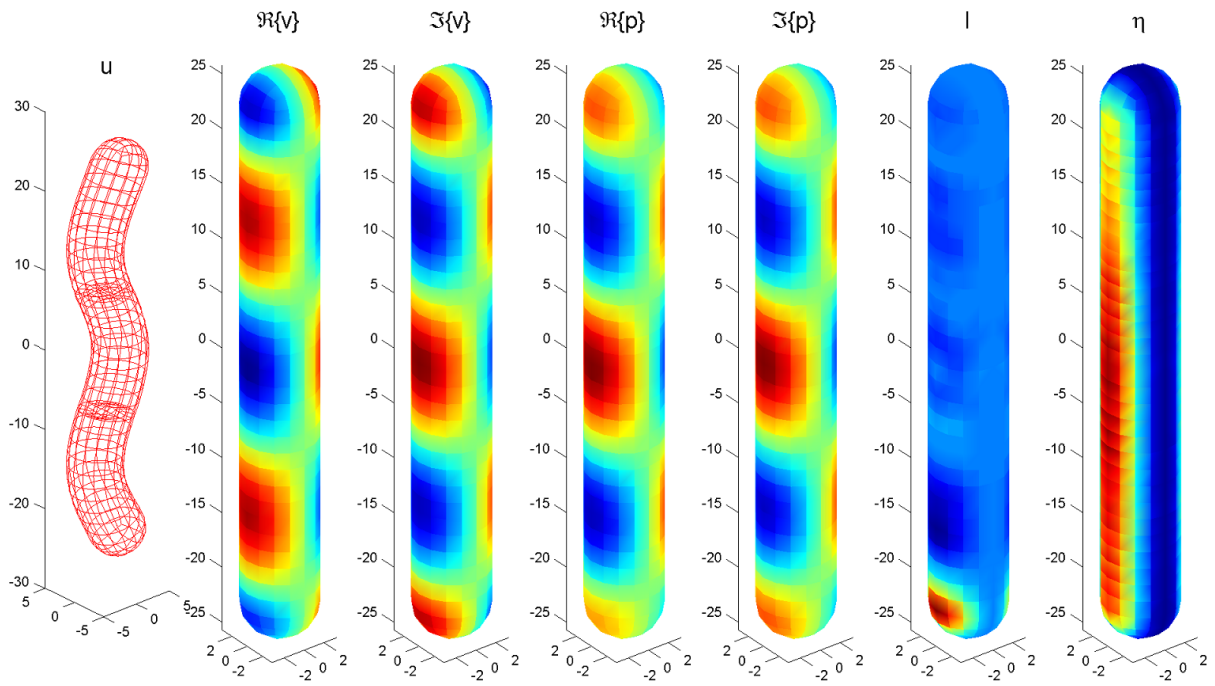
Figure 1 – Number of integration points per element as a function of distance between collocation points and the element

difficult for adjacent areas that have areas with active acoustic intensity of opposite signs to exchange acoustic energy.

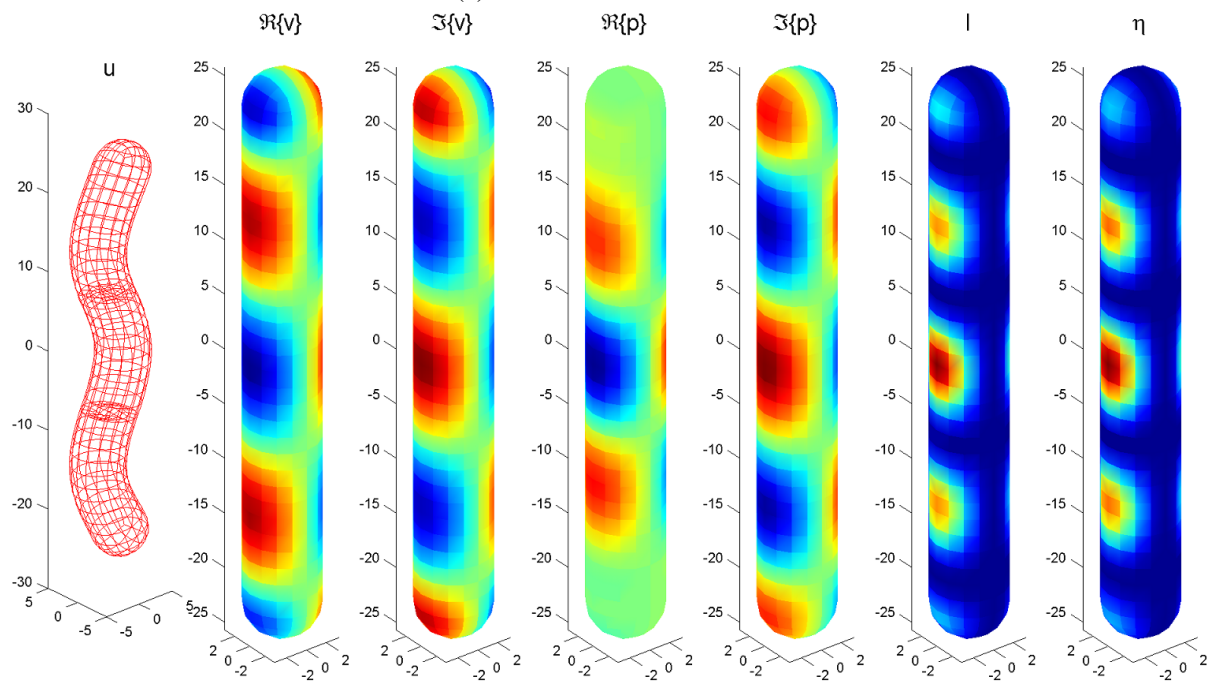
Acoustic radiation efficiencies calculated using Eq. (6) are presented in Figures 3 and 4 using the number of integration points given by sets A and B, respectively. In both figures, the acoustic radiation efficiencies of the first ten acoustic radiation modes, using both coarse and fine discretized meshes, are shown. Figure 3 shows the acoustic radiation efficiencies of the first ten acoustic radiation modes with coarse and fine discretizations, based on integration points in set A between 0.01 Hz and 100 Hz. The top line represents the first acoustic radiation mode with the highest acoustic radiation efficiency for the entire frequency range. The radiation efficiencies gradually decrease when the frequency is reduced. The remaining radiation efficiencies converge to approximately 10^{-12} in Figure 3(a). In theory, the radiation efficiencies should continue to decrease in a straight line when presented on a logarithmic scale. The boundedness of the radiation efficiencies at $\sigma = 10^{-12}$ as the efficiency decreases towards low frequencies is due to numerical limitations. Using a fine discretization in Figure 3(b), the boundedness of the acoustic radiation efficiencies still occurs at 10^{-12} . Figure 4 shows that the acoustic radiation efficiencies approach to approximately 10^{-16} using a higher number of integration points in set B. Similar to Figure 3, in Figure 4 there is no apparent difference between a coarse and a fine discretization.

The sound power of the first three bending modes calculated using both acoustic intensity given by Eq. (3) and surface contributions given by Eq. (7), for a frequency range from 0.01 Hz to 100 Hz, are compared in Figure 5. The numerical model uses fine discretization and integration points in set A. Similar to the acoustic radiation efficiencies, Figure 5(a) shows that the sound power gradually increases as the frequency increases. The first bending mode consistently contributes more sound power than the other two bending modes. The sound power based on both methods are very similar and show the same trend. The differences between the two methods shown in Figure 5(b) range from approximately 70% to 140% up to 10 Hz. The differences converge to zero after around 10 Hz. The sound power calculated using the acoustic intensity and surface contribution methods, as well as their differences, are presented in Figure 6 using integration points in set B. Figure 6(a) shows that the sound power becomes less than 10^{-25} at 0.01 Hz. Figure 6(b) shows that the difference between the two methods converge after around 0.2 Hz.

As shown in Figures 3 and 4, when increasing the number of integration points, the acoustic radiation efficiencies converge from 10^{-12} to 10^{-16} . Similar to the acoustic radiation efficiencies, the results from eigenvalue decomposition also affect the surface contributions and hence the radiated sound power based on the surface contribution method. Therefore, more integration points are recommended for the surface contribution method at low frequencies. However, more integration points require significantly more computing process to build the boundary element matrices. For more complex geometries, less discretization and necessary number of integration points are suggested at low frequencies.



(a) Sound radiation at 1 Hz



(b) Sound radiation at 100 Hz

Figure 2 – Sound radiation for the third bending mode of the fluid-loaded cylindrical shell

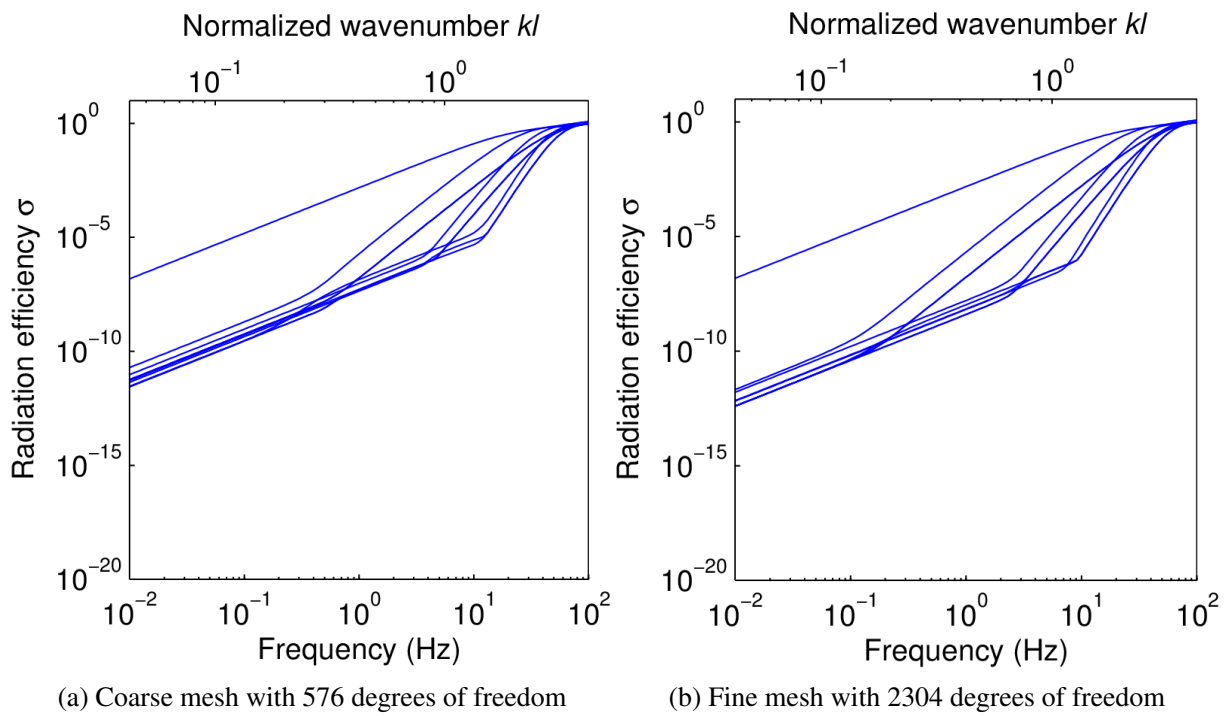


Figure 3 – Radiation efficiency of the first ten acoustic radiation modes using the number of integration points given by set A

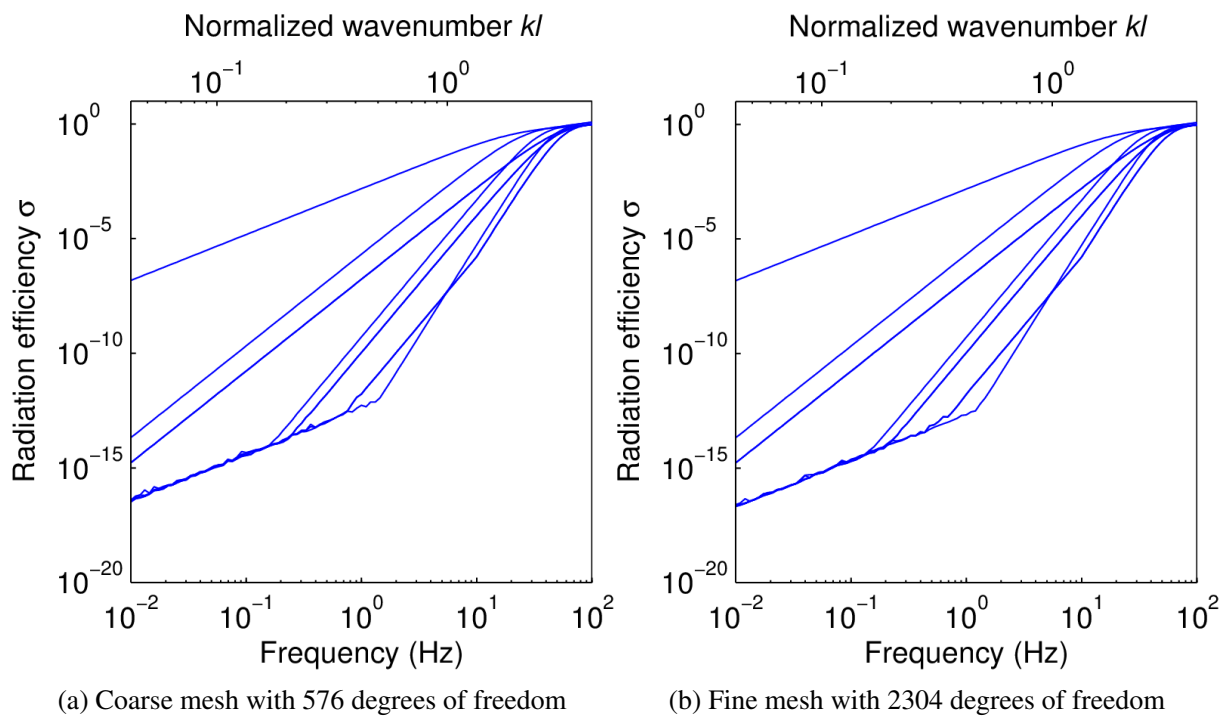


Figure 4 – Radiation efficiency of the first ten acoustic radiation modes using the number of integration points given by set B

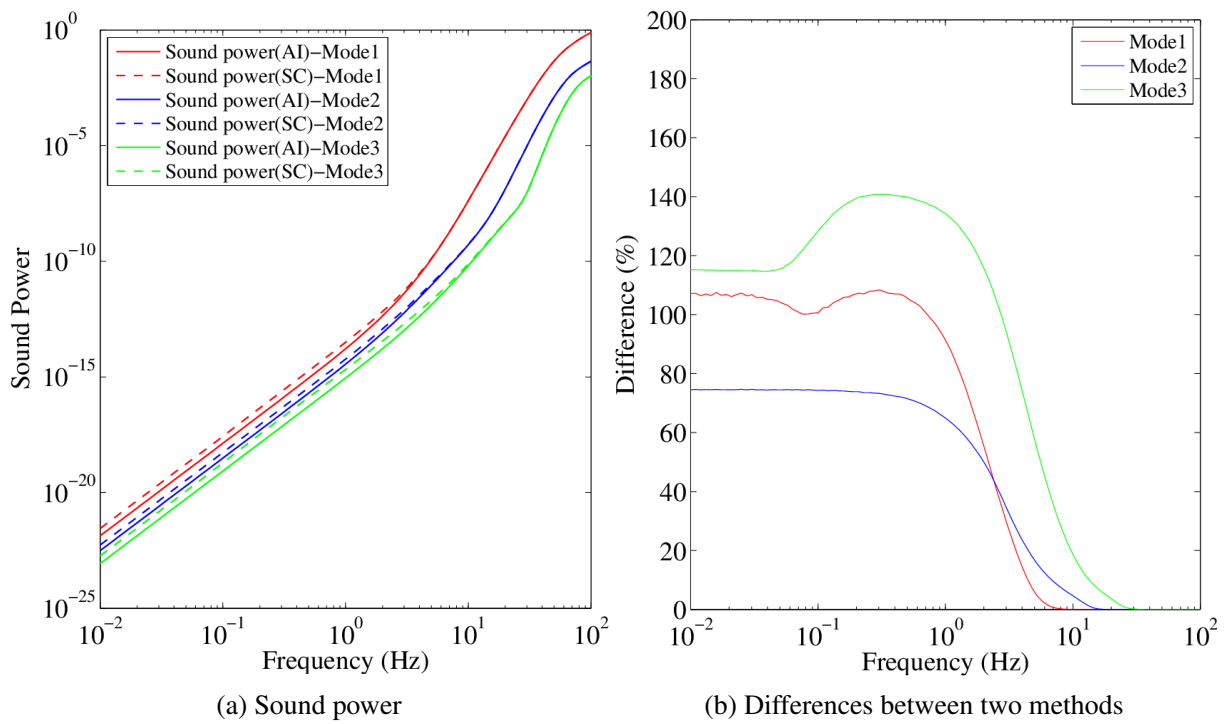


Figure 5 – Sound power from active intensity and surface contribution methods and the differences using the number of integration points given by set A

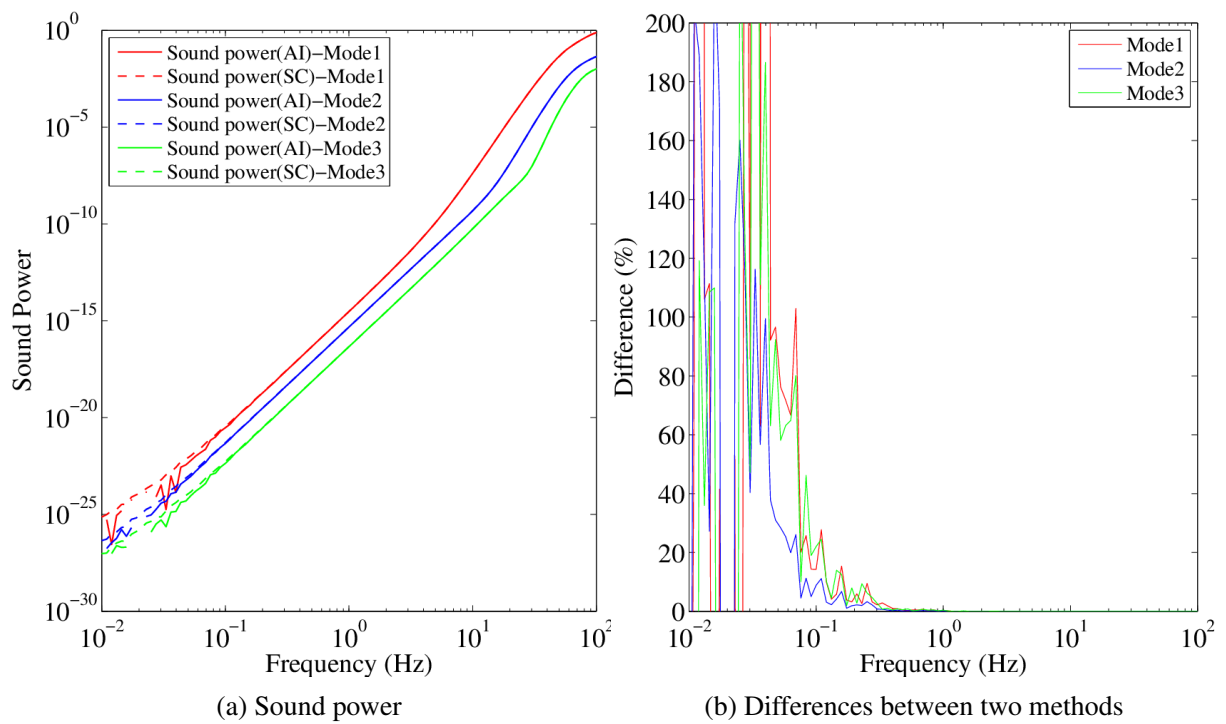


Figure 6 – Sound power from active intensity and surface contribution methods and the differences using the number of integration points given by set B

4. CONCLUSIONS

The surface contribution method applied to a fully coupled finite element/boundary element model of a cylindrical shell with hemispherical end closures and submerged in water has been presented. The radiation patterns of surface contributions and acoustic intensity have been compared at different frequencies. The sound power of the first three bending modes based on both the surface contribution method and active intensity have been compared. The acoustic radiation efficiencies and surface contributions calculated using two different sets of integration points are presented. When the number of integration points for the boundary element matrices increases, the accuracy of the radiation efficiencies increases at low frequencies. As a result, the frequency at which the sound power based on the active intensity and surface contribution method converges, is reduced. This work shows that the surface contribution method can be applied at low frequencies.

5. ACKNOWLEDGMENT

The first author gratefully acknowledges the financial assistance provided by the Australian Acoustical Society NSW Division to attend the Inter-Noise 2014 conference.

REFERENCES

1. Borgiotti GV. The power radiated by a vibrating body in an acoustic fluid and its determination from boundary measurements. *J Acoust Soc Am.* 1990;88(4):1884–1893.
2. Maidanik G. Response of ribbed panels to reverberant acoustic fields. *J Acoust Soc Am.* 1962;34(6):809–826.
3. Photiadis DM. The relationship of singular value decomposition to wave-vector filtering in sound radiation problems. *J Acoust Soc Am.* 1990;88(2):1152–1159.
4. Sarkissian A. Acoustic radiation from finite structures. *J Acoust Soc Am.* 1991;90(1):574–578.
5. Cunefare KA, Currey MN. On the exterior acoustic radiation modes of structures. *J Acoust Soc Am.* 1994;96(4):2302–2312.
6. Snyder SD, Tanaka N. Calculating total acoustic power output using modal radiation efficiencies. *J Acoust Soc Am.* 1995;97(3):1702–1709.
7. Marburg S, Lösche E, Peters H, Kessissoglou N. Surface contributions to radiated sound power. *J Acoust Soc Am.* 2013;133(6):3700–3705.
8. Williams EG. Convolution formulations for non-negative intensity. *J Acoust Soc Am.* 2013;134(2):1055–1066.
9. Williams EG. Supersonic acoustic intensity. *J Acoust Soc Am.* 1995;97(1):121–127.
10. Williams EG. Supersonic acoustic intensity on planar sources. *J Acoust Soc Am.* 1998;104(5):2845–2850.
11. Peters H, Kessissoglou N, Marburg S. Modal decomposition of exterior acoustic-structure interaction problems with model order reduction. *J Acoust Soc Am.* 2014;135(5):2706–2717.
12. Peters H, Marburg S, Kessissoglou N. Structural-acoustic coupling on non-conforming meshes with quadratic shape functions. *Int J Numer Meth Eng.* 2012;91(1):27–38.
13. Marburg S, Nolte B. *Computational Acoustics of Noise Propagation in Fluids - Finite and Boundary Element Methods.* Berlin, Heidelberg: Springer-Verlag; 2008.
14. Wu TW. *Boundary Element Acoustics - Fundamentals and Computer Codes.* UK: WIT Press; 2000.
15. Elliott SJ, Johnson ME. Radiation modes and the active control of sound power. *J Acoust Soc Am.* 1993;94(4):2194–2204.
16. Peters H, Kessissoglou N, Marburg S. Enforcing reciprocity in numerical analysis of acoustic radiation modes and sound power evaluation. *J Comput Acoust.* 2012;20(03):1250005.
17. Marburg S, Schneider S. Influence of element types on numeric error for acoustic boundary elements. *J Comput Acoust.* 2003;11(03):363–386.
18. Telles JCF. A self-adaptive co-ordinate transformation for efficient numerical evaluation of general boundary element integrals. *Int J Numer Meth Eng.* 1987;24(5):959–973.